Correlation analysis between plasmon field distribution and sensitivity enhancement in reflection- and transmission-type localized surface plasmon resonance biosensors

Nak-Hyeon Kim, Woo Kyung Jung, and Kyung Min Byun*

Department of Biomedical Engineering, Kyung Hee University, Yongin 446-701, South Korea

*Corresponding author: kmbyun@khu.ac.kr

Received 29 April 2011; revised 30 June 2011; accepted 5 July 2011;
posted 6 July 2011 (Doc. ID 146512); published 26 August 2011

We examine the correlation between the plasmon field distribution and the sensitivity enhancement for both reflection- and transmission-type localized surface plasmon resonance (LSPR) biosensors with surface-relief gold nanogratings. In our calculation, the near-field characteristics are obtained from the finite-difference time-domain method and compared with the refractive index sensitivity as a unit target sample moves along the sensor surface. The numerical results show that the highest enhancement of sensitivity is found at the lower grating corners where an interplay between the target sample and the locally enhanced field can occur efficiently. This study suggests that, by localizing biomolecular interactions to the highly enhanced field, we can achieve a significantly improved LSPR detection with high sensitivity and a great linearity in a wide dynamic range.

OCIS codes: 050.2770, 280.4788, 240.6680.

1. Introduction

The surface plasmon resonance (SPR) phenomenon has been extensively utilized for monitoring biomolecular interactions on a noble metal film [1]. Surface plasmons (SPs) are collective charge oscillations propagating along the interface between a metal and a dielectric. The amplitude of SP waves generally reaches a maximum under the condition that the momentum matching between an incident photon and an SP is achieved. In SPR-based optical biosensing, we can analyze the adsorption of target analytes coupled with surface-immobilized ligands by tracking the change in the resonance position. A conventional SPR biosensor based on the standard Kretschmann configuration generally works as a reflection type in the sense that a photodetector measures the reflected light [2]. For this scheme, the resonance appears as a deep absorption band in the reflectivity versus incidence angle or wavelength.

Contrary to the propagating SP waves, metallic nanostructures lead to a substantial enhancement of local electromagnetic fields as a result of the strong light absorption and scattering, called localized SPs (LSPs) [3]. The frequency of the LSP resonance (LSPR) band is the characteristic of the material, size, shape, and distribution of the nanostructure as well as its surrounding local environments. Since the experimental setup, often using a wavelength interrogation scheme, employs a white light with a normal incidence and the LSPR spectrum is obtained by delivering the transmitted light onto a spectrometer via an objective lens and optical fibers, its sensing configuration belongs to a transmission type [4]. While the LSPR biosensor generally suffers from relatively lower sensor sensitivity due to the resolution limit of the spectroscopy instrumentation and the restricted sensing range of a few tens of nanometers, an exposure of biomolecular

0003-6935/11/254982-07$15.00/0

interactions to highly localized fields, called hot spots, may yield a stronger resonance shift, thereby significantly enhancing the sensor sensitivity [5,6]. Recent comparison studies between SPR and LSPR biosensors demonstrated that their overall sensitivities are approximately equivalent for unit volume of target analytes [7,8].

Among various plasmonic biosensing schemes, the approach on which we have focused is to enhance the SPR detection by incorporating LSPR-based surface-relief nanostructures such as gold nanogratings and nanoholes [9,10]. The improved sensitivity based on the surface nanostructure is associated with an increase of reaction area and, more importantly, a strong interplay of target analytes with the excited LSP modes. In other words, it has been supposed that when a biomolecular interaction is exposed to highly localized fields, the resonance shift as a result of the biointeraction would be stronger [11]. While the sensitivity may not be governed by only one factor, our theoretical and experimental results have verified that this effect may be true.

Despite such a critical contribution of the resonant LSP modes to sensitivity enhancement, a more in-depth investigation on the correlation between the local field amplification and the sensor sensitivity has not been addressed yet. Thus, in this study, we intend to demonstrate how to make the most of the nanostructured plasmonic substrates by coinciding the localized target molecules and the evanescent near fields. Instead of a simple use of metallic nanostructures, selective target localization in the local hot spots would open up a possibility of maximizing the detection sensitivity.

2. Numerical Model

Optical characteristics of subwavelength metallic nanogratings can be obtained numerically using rigorous coupled-wave analysis (RCWA) [12–14]. RCWA has been successfully applied to describing experimental results of periodic nanostructures [15,16]. In this study, convergence of RCWA is achieved by including 30 space harmonic orders in the computation. In addition, the finite-difference time-domain (FDTD) method has been used to visualize the near-field distribution. The minimum grid size for the FDTD is set to be 0.5 nm.

Schematic diagrams of gold-nanograting-based LSPR configurations are shown in Fig. 1. First, for a reflection-type LSPR biosensor, periodic nanogratings patterned on a flat gold film with a thickness of $d_f = 40$ nm support the excitation of LSP modes. Rectangular gold gratings with a period of $\Lambda = 60$ nm have a width of 30 nm and a thickness of $d_g = 10$ nm. The whole gold surface is assumed to be open to an immobilization of ligands with which the target molecules combine. In particular, while not shown in the illustration, a single biomolecule complex is modeled as a 2 nm × 2 nm dielectric medium per period to investigate the influence of target localization on the sensor sensitivity. In this model, its change in optical

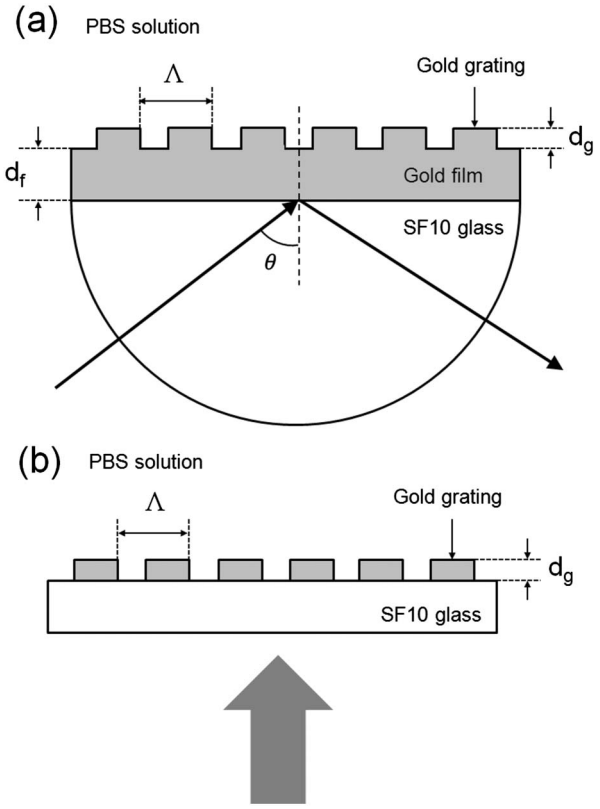

Fig. 1. Schematic of (a) reflection-type and (b) transmission-type LSPR sensing configurations. For reflection type, TM-polarized light with $\lambda = 633$ nm is incident through gold/SF10 substrate with an angle of θ. Gold nanogratings with a thickness of $d_g = 10$ nm are regularly patterned on the planar gold film (thickness $d_f = 40$ nm) in PBS environments. The grating structure of a rectangular profile has a period of $\Lambda = 60$ nm and a duty cycle = 0.5. For transmission type, TM-polarized white light source is normally incident to the gold nanogratings directly deposited on SF10 glass substrate. Geometric parameters of a gold nanograting are the same as those for the reflection type.

property during the binding process is simulated as the refractive index change ranging from 1.40 for ligand immobilization to 1.60 for target adsorption in a phosphate-buffered saline (PBS) solution whose refractive index is 1.33. A polarized light at $\lambda = 633$ nm is incident through the gold/SF10 substrate and the reflectance curve is obtained from RCWA calculations as the light incidence is scanned with an angular resolution of 0.01°.

Second, for transmission type one, we consider gold nanogratings directly deposited on an SF10 substrate as presented in Fig. 1(b). The geometric parameters of gold nanogratings and biomolecule complexes are the same as those for the reflection type. TM-polarized light, the electric field of which oscillates in parallel to the grating vector, is normally incident to the grating structure surrounded by PBS solution. To calculate the extinction characteristics of the transmitted light, the wavelength is scanned with a spectral resolution of 0.1 nm. In both cases of reflection and transmission types, the frequency-dependent permittivities of SF10 and gold are taken from Ref. [17].

3. Results and Discussion

A. Reflection-Type LSPR Biosensor

Let us start by considering a conventional SPR structure without gold nanogratings. While the results are not illustrated here, when a refractive index of 2 nm × 2 nm dielectric square with a periodicity of $\Lambda = 60$ nm varies from 1.40 to 1.60, the SPR angles are equal to 59.25° and 59.27° regardless of adsorption site, and the net shift is 0.02°. In fact, actual biomolecular interactions take place at the whole sensor surface and, thus, the formation of a uniform biolayer and the estimation of the sensitivity in response to its small change in refractive index seem reasonable. However, the amount of target molecules that is needed to achieve a resonance shift can be varied when surface-relief nanostructures are applied to the sensor substrate. In other words, since a contrast of the total amount of target adsorption needs to be eliminated in evaluating the contribution of local field enhancement to the sensitivity characteristic, the sensitivity comparison based on unit target volume would be more appropriate. Hence, as a performance measure, we have employed the sensitivity enhancement factor per unit target volume (SEF_{UTV}), which is a ratio of SPR shift due to a refractive index change in unit volume of 2 nm × 2 nm on an LSPR substrate to that of a thin-film-based SPR structure. As a result, SEF_{UTV} excludes the effect of a surface reaction area on the sensitivity and directly addresses the contribution of LSP modes to the sensitivity improvement.

In what follows, the shift of the resonance angle by an adsorption of the unit dielectric element is calculated in a reflection-type LSPR structure when the dielectric moves along the grating surface presented in Fig. 1(a). Several notes are worth a look in the results presented in Fig. 2. First, overall trends of a greater resonance shift in the vicinity of the grating corners are obvious. When the refractive index changes from 1.40 to 1.60, the highest SPR angle shift is obtained to be 0.39° at the two lower vertices of a gold nanograting, which corresponds to a sensitivity = 1.95°/refractive index unit (RIU) and an $SEF_{UTV} = 19.5$. Also, at the upper grating corners, a few SEF_{UTV} peaks that show a significant resonance change of more than 0.25° are found. Interestingly, among the three immobilization sites of nanograting top, sidewall, and bottom, the sensitivity enhancement associated with the target localized on the grating sidewalls is by far the largest. On the other hand, the dielectric element present on the nanograting top and bottom produces a minor change in resonance angle except at the grating corner and the lowest shift is determined as 0.01°, half that of a conventional SPR substrate, on a unit volume basis. We believe that this nonuniform sensitivity characteristic is strongly related to an inhomogeneous distribution of the field intensity over the LSPR sensor surface.

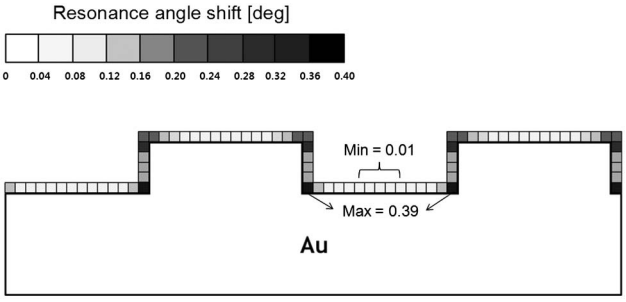

Fig. 2. Resonance angle shift characteristic for reflection-type LSPR substrate when a 2 nm × 2 nm dielectric element moves along the sensor surface. When its refractive index increases from 1.40 to 1.60, the highest sensitivity is obtained to be 1.95°/RIU at the lower corners of a gold nanograting and the minimum sensitivity of 0.05°/RIU is found at the center areas between gold nanogratings.

Additionally, in comparison with the case without target localization in which a refractive index of a 2 nm thick dielectric layer covering the entire surface of a planar SPR substrate increases from 1.40 to 1.60, the resonance shift of 0.34° is found numerically and is smaller than the maximum resonance angle shift of 0.39° obtained from a unit dielectric element attached to a lower grating corner. This supports an intriguing postulation that one can realize an extremely sensitive LSPR biosensor by guiding the immobilization of ligands selectively onto the more sensitive region, such as nanograting corners and sidewalls.

Next, in order to confirm the correlation between the refractive index sensitivity and the local field enhancement, we visualize the electromagnetic fields near the sensor surface based on the FDTD method. Figure 3 shows the field distribution of E_X at a resonance incidence of $\theta = 73.36°$ and provides horizontal and vertical field amplitudes at the gold nanograting. Obviously, the metallic gratings redistribute the propagating SP waves such that higher field strength is found at the grating corners. The

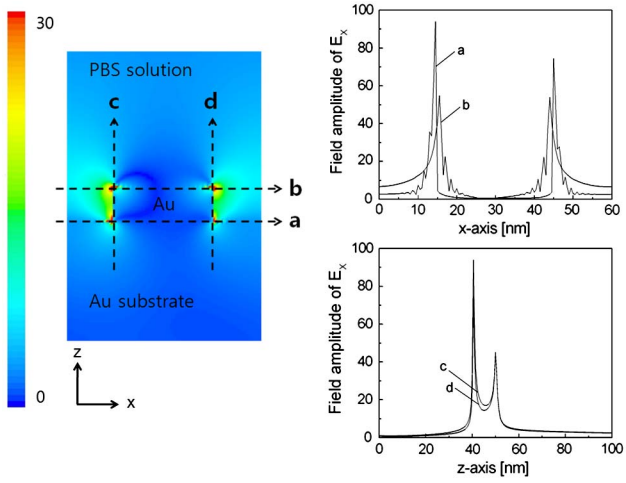

Fig. 3. (Color online) Horizontal and vertical field distributions of E_X for reflection-type LSPR structures with a gold grating of $\Lambda = 60$ nm, duty cycle = 0.5, and $d_g = 10$ nm. The two-dimensional image obtained from the FDTD calculation is normalized by the field amplitude of 30.

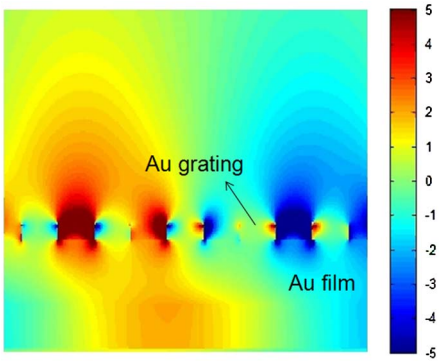

Fig. 4. (Color online) Real part of the field component E_X in the same LSPR structure as Fig. 3. Media 1 shows time-varying near-field characteristics induced by a gold nanograting and a planar gold film when the field amplitude is normalized by a value of 5.

FDTD calculation presents that primary peaks are located on the two lower edges of the nanograting and the secondary peaks on the upper sides. On the assumption of an incident light of unit amplitude, the maximum field amplitudes obtained are $E_X = 94.0$, $H_Y = 12.8$, and $E_Z = 65.0$, respectively. Since locally enhanced plasmon is distributed at a very short distance from the substrate and its amplitude decays exponentially when one moves further away from the grating surface, individual plasmon peaks associated with the four grating corners can be regarded as resonant LSP modes [18].

It is also worth keeping an eye on where these hot spots occur. Figure 3 shows that all the maximum fields are located within 1 nm of the surface in the vicinity of grating vertices. Because of this field enhancement, target analytes adsorbed at the nanograting corners participate more vigorously on average than those on the other grating regions, leading to the most prominent improvement of sensitivity, as shown in Fig. 2. Among the four vertices of a gold nanograting, relatively larger field amplification is found at the lower grating edges where the excited LSP modes can be partially absorbed by a planar gold film. Despite such possible attenuation, the strongest LSP fields obtained at the lower grating edges lead to the largest resonance shift through an efficient interplay between the target analytes with a unit volume and the enhanced LSPs. This interpretation supports a strong correlation between the plasmon field distribution and the spatial sensitivity profile.

Further, it is interesting in Fig. 3 that the grating sidewalls with a larger field amplification tend to produce a higher sensitivity. Since more amplified fields appear at the grating sidewalls, constructive interactions between the excited LSP modes and the target on the sidewalls yield an enhanced sensitivity by more than 6 times, compared to those on the grating top and bottom. In short, the selective target adsorption overlapping the main resonances at the grating edges and their adjacent areas of grating sidewalls may play an important role in achieving a notable improvement of the refractive index sensitivity.

The results of another FDTD shown in Fig. 4 imply time-varying characteristics of LSP modes at the gold gratings in the same LSPR structure as Fig. 3. In this computation, the real part of the field component E_X is normalized by a value of 5. Media 1, linked to Fig. 4, exhibits how the proposed LSPR substrate produces local plasmon fields at the grating corners via the coupling with propagating SPs. For more efficient excitation of the highest LSP fields at the lower edges, an intermediate dielectric spacer between the gold nanograting and the underlying gold film could be used, while the difficulty in an actual fabrication may increase [19].

B. Transmission-Type LSPR Biosensor

In contrast to the reflection-type LSPR biosensor, the transmission-type one is fully based on the LSP modes; thus, its performance is free from an interplay with a thin metal film supporting a propagating SP wave. Moreover, due to the compact optical setup based on wavelength scanning at normal incidence, its important characteristic is the capability for high-throughput monitoring, for example in DNA research and proteomics for which thousands of binding interactions should be examined rapidly [20]. For the proposed transmission-type LSPR configuration shown in Fig. 1(b), extinction spectra for periodic gold nanogratings are calculated to quantify the sensor sensitivity with respect to changes in the refractive index of the 2 nm × 2 nm dielectric sample. Optical extinction is defined as $-\log(T)$, where T denotes the transmittance as a function of the light's wavelength. The resonance wavelength shift is evaluated as the dielectric square moves along the LSPR substrate with a gold nanograting of a period of $\Lambda = 60$ nm, $d_g = 10$ nm, and a duty cycle = 0.5.

In Fig. 5, the overall trends are consistent with those for the reflection type. The refractive index change occurring at the grating corners produces a significant LSPR shift and the highest refractive index sensitivities are obtained to be 5.0 nm/RIU at

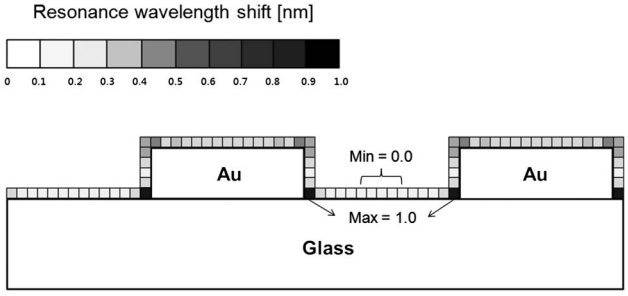

Fig. 5. Resonance wavelength shift characteristic for transmission-type LSPR substrate when a 2 nm × 2 nm dielectric element moves along the sensor surface. When its refractive index increases from 1.40 to 1.60, the highest sensitivity is obtained to be 5.0 nm/RIU at the lower corners of a gold nanograting and the minimum sensitivity of 0.0 nm/RIU is found at the center areas between gold nanogratings.

the lower grating corners. Also, as the second sensitivity peaks of 2.5 nm/RIU are found near the upper grating corners, it is obvious that the binding events associated with the localization at the grating corners make a significant contribution to achieving a high sensitivity. On the other hand, the sidewall effect does not appear prominent in the transmission type, and, in particular, no refractive index shift is found when the dielectric element is deposited on a glass substrate and is more than 10 nm apart from the gold gratings. We suppose that the evanescent field produced at the analyte interface is responsible for this nonuniform distribution of the sensor sensitivity in the same way as the reflection-type LSPR substrate.

To verify the correlation between the refractive index sensitivity and the local plasmon field, we provide horizontal and vertical field amplitudes of E_X at a normal incidence as presented in Fig. 6. The FDTD results show that the two main resonances are found on the lower corners of the nanograting and the secondary peaks on the two upper corners. Of importance is that the field distribution is highly consistent with the sensitivity profile of Fig. 5. On the assumption of an incident light of a unit amplitude, maximum field amplitudes are obtained as $E_X = 30.3$, $H_Y = 4.0$, and $E_Z = 23.2$. Among individual hot spots associated with the four grating corners, maximal field amplification is found at the lower grating edges in perfect symmetry. Hence, due to the largest field enhancement and its strong interplay with the dielectric sample, we can achieve the greatest sensitivity at the lower grating corners for the unit sample volume.

Media 2, linked to Fig. 7, shows the generation of LSP modes in the gold nanogratings at a normal incidence of $\lambda = 632.8$ nm. While we cannot clearly identify the resonant LSP mode at each grating corner due to its extremely short decay length, we can confirm the coupling of an incidence beam with the gold nanogratings in the near-field region. From the FDTD results in Figs. 3 and 6, the decay length of the LSP mode in the transmission-type LSPR substrate is much shorter than that of the reflection-type one. In addition, as no significant field amplification is found at the grating sidewalls, the refractive index sensitivity on the grating sidewall is actually modest compared to those of the other grating sides. When the field amplitude is normalized by 5, readers may notice that the plasmon fields at the grating sidewalls in Fig. 7 are not as dominant as the results for the reflection type in Fig. 4.

Consequently, unlike the reflection-type LSPR biosensor based on the interaction between the propagating SP and LSP modes, the field enhancement for the transmission type is simply governed by the resonant LSP characteristics. Based on this plasmonic interpretation for the LSPR sensitivity concept, we can develop a simple but efficient LSPR biosensing scheme by incorporating a pointed metallic nanostructure on a glass substrate and guiding the surface reactions selectively onto the sharp point where the field intensity is greatest. Recently, rapid development of nanofabrication techniques made it possible to realize a highly sensitive LSPR sensor with high-density arrays of metallic nanostructure with a pointed shape [21,22]. For example, Kontio *et al.* demonstrated that nanoimprint lithography combined with electron-beam evaporation provides a cost-efficient, rapid, and reproducible method to fabricate conical nanostructures with very sharp tips on flat surfaces in high volumes [22]. In particular, it is noteworthy that strong local fields at the tips enhanced the second harmonic generation by over 2 orders of magnitude compared with nonsharp nanotips. On the other hand, when it is not practically easy to fabricate the sharp edges or to guide the target molecules into the hot spots, another possibility is to obtain a large volume with a relatively large field enhancement through a direct interaction between plasmonic structures [23]. Design optimization of plasmonic substrates for larger field volume with a stronger enhancement can be an effective

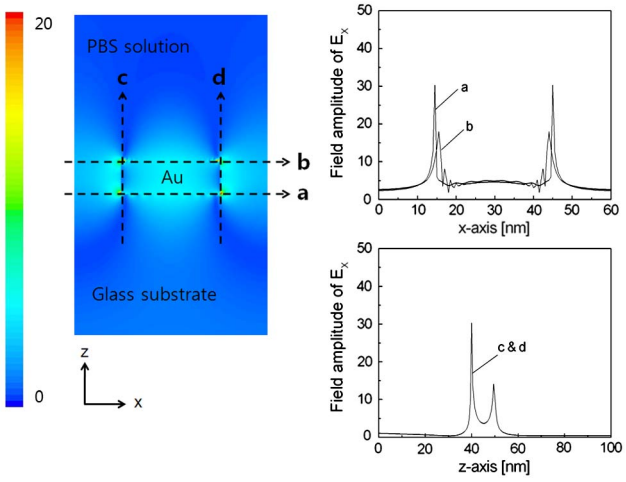

Fig. 6. (Color online) Horizontal and vertical field distributions of E_X for transmission-type LSPR structures with a gold grating of $\Lambda = 60$ nm, duty cycle = 0.5, and $d_g = 10$ nm. The two-dimensional image obtained from the FDTD calculation is normalized by the field amplitude of 20.

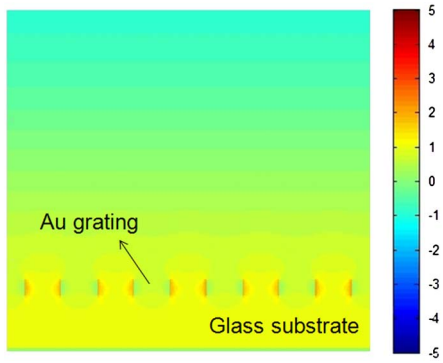

Fig. 7. (Color online) Real part of the field component E_X in the same LSPR structure as Fig. 6. Media 2 shows time-varying near-field characteristics induced by a gold nanograting when the field amplitude is normalized by a value of 5.

approach for developing a high-sensitivity LSPR biosensor.

C. Linear Sensing Performance

The target attachment to a lower grating edge where the maximum resonance shift occurs has been proposed as an optimal localization and is now evaluated in terms of the linearity, which is another important sensing performance. For reflection and transmission LSPR types, resonance angle or wavelength is calculated as a function of the refractive index, which ranges from 1.33 (i.e., without a binding event in PBS solution) to 1.60 in accordance with the concentration of adsorbed analytes. This wide refractive index change is intended to consider the whole binding process including both the adsorption of receptors and the adsorption of target analytes. Figure 8 shows that, for reflection-type LSPRs, the resonance angle shifts from 73.46° to 73.85° as a refractive index of the dielectric square varies from 1.40 to 1.60. In particular, from the inset of Fig. 8, a linear relationship over the whole range of refractive indices is evident with $R = 0.99746$ (R is the correlation coefficient that denotes the linearity obtainable in the sensor performance). Also, extinction spectra of transmission-type LSPR configurations are presented in Fig. 9 and the inset of linear regression analyses demonstrates that the resonance shift in response to an increase in the refractive index is extremely linear with $R = 0.99881$. As a result, we confirm that the selective target localization can be an effective way to realize an enhanced LSPR detection with high sensitivity and a great linearity in a wide dynamic range.

Finally, in regard to actual implementation, selective adsorption of biomolecules can be achieved by opening a small area of ultrathin dielectric mask layers through a slanted evaporation technique [24]. Since a lower corner of the gold nanograting where the mask layer is not covered is exposed to the receptors in a closed fluidic channel, both ligands and target analytes can be better localized. While realizing a thin dielectric mask layer in a reproducible manner still remains a challenge, the relevant experimental work is currently under way using nanoimprint lithography and angled evaporation techniques.

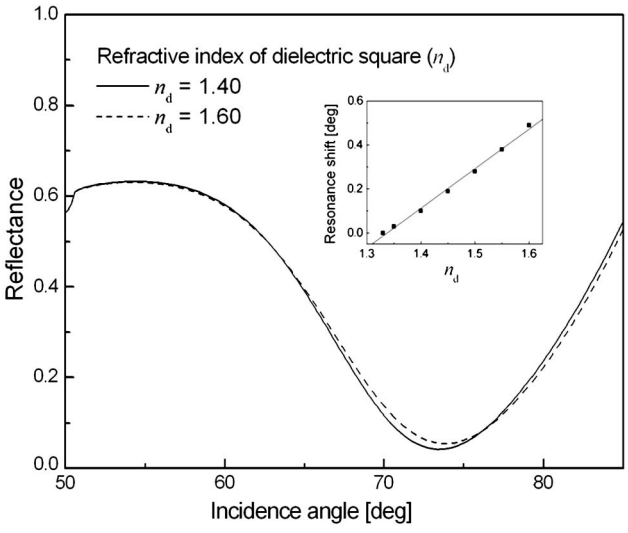

Fig. 8. Reflectance curves of the reflection-type LSPR structure as a refractive index n_d of the dielectric element increases from 1.40 to 1.60. The inset shows the linear regression analysis between n_d and the resonance angle shift.

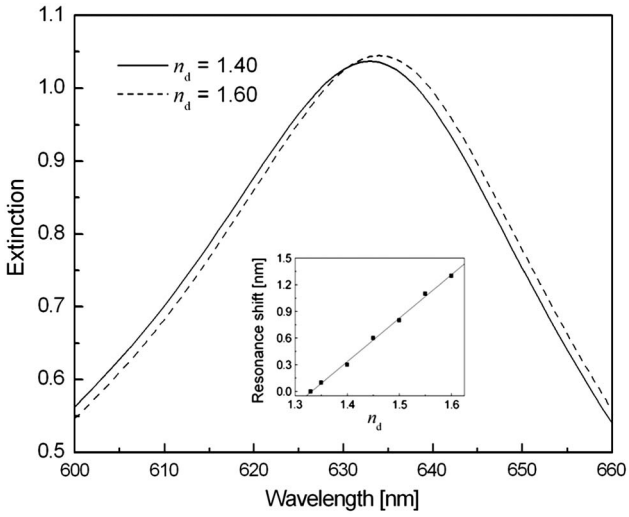

Fig. 9. Extinction spectra of the transmission-type LSPR structure as a refractive index n_d of the dielectric element increases from 1.40 to 1.60. The inset shows the linear regression analysis between n_d and the resonance wavelength shift.

4. Conclusion

In this study, we have investigated the correlation between the plasmon field distribution and the refractive index sensitivity using surface-relief gold nanogratings. For both reflection- and transmission-type LSPR structures, our numerical results show that the remarkable improvement in surface sensitivity is highly associated with the localized field amplitude of hot spots occurring at the grating corners. While this study is theoretical, the result is quite noticeable in the sense that it shows the possibilities of enhancing the sensitivity by 1 order of magnitude for the unit's target volume and increasing the sensor efficiency by preventing the target molecules from being wasted in the weak field. In an actual sensing application, as the guided ligand immobilization allows the target analytes to be targeted to the region with high field intensity, target molecules, especially those with a very low concentration, can produce an appreciable resonance shift. Finally, including the limit of detection, which is another important performance indicator representing the smallest change in the refractive index that produces a detectable change in the sensor output [25], our subsequent studies will have more in-depth discussions on the overall sensor performance after a further structural optimization of the proposed reflection- and transmission-type LSPR structures.

This work was supported by the Korea Science and Engineering Foundation (KOSEF) grant funded by the Korean government (MEST) (2011-0005137).

References

1. J. Homola, S. S. Yee, and G. Gauglitz, "Surface plasmon resonance sensors: review," Sens. Actuators B **54**, 3–15 (1999).
2. E. Kretschmann, "Decay of non radiative surface plasmons into light on rough silver films. comparison of experimental and theoretical results," Opt. Commun. **6**, 185–187 (1972).
3. E. Hutter and J. H. Fendler, "Exploitation of localized surface plasmon resonance," Adv. Mater. **16**, 1685–1706 (2004).
4. J. Zhao, X. Zhang, C. R. Yonzon, A. J. Haes, and R. P. Van Duyne, "Localized surface plasmon resonance biosensors," Nanomedicine **1**, 219–228 (2006).
5. J. N. Anker, W. P. Hall, O. Lyandres, N. C. Shah, J. Zhao, and R. P. Van Duyne, "Biosensing with plasmonic nanosensors," Nat. Mater. **7**, 442–453 (2008).
6. A. J. Haes, S. Zou, G. C. Schatz, and R. P. Van Duyne, "Nanoscale optical biosensor: short range distance dependence of the localized surface plasmon resonance of noble metal nanoparticles," J. Phys. Chem. B **108**, 6961–6968 (2004).
7. A. D. McFarland and R. P. Van Duyne, "Single silver nanoparticles as real-time optical sensors with zeptomole sensitivity," Nano Lett. **3**, 1057–1062 (2003).
8. A. J. Haes and R. P. Van Duyne, "A unified view of propagating and localized surface plasmon resonance biosensors," Anal. Bioanal. Chem. **379**, 920–930 (2004).
9. K. Kim, D. J. Kim, S. Moon, D. Kim, and K. M. Byun, "Localized surface plasmon resonance detection of layered biointeractions on metallic subwavelength nanogratings," Nanotechnology **20**, 315501 (2009).
10. S. A. Kim, K. M. Byun, K. Kim, S. M. Jang, K. Ma, Y. Oh, D. Kim, S. G. Kim, M. L. Shuler, and S. J. Kim, "Surface-enhanced localized surface plasmon resonance biosensing of avian influenza DNA hybridization using subwavelength metallic nanoarrays," Nanotechnology **21**, 355503 (2010).
11. K. M. Byun, S. M. Jang, S. J. Kim, and D. Kim, "Effect of target localization on the sensitivity of a localized surface plasmon resonance biosensor based on subwavelength nanostructures," J. Opt. Soc. Am. A **26**, 1027–1034 (2009).
12. M. G. Moharam and T. K. Gaylord, "Rigorous coupled-wave analysis of metallic surface-relief gratings," J. Opt. Soc. Am. A **3**, 1780–1787 (1986).
13. L. Li, "Multilayer modal method for diffraction gratings of arbitrary profile, depth, and permittivity," J. Opt. Soc. Am. A **10**, 2581–2591 (1993).
14. L. Li and C. W. Haggans, "Convergence of the coupled-wave method for metallic lamellar diffraction gratings," J. Opt. Soc. Am. A **10**, 1184–1189 (1993).
15. Y. Kanamori, K. Hane, H. Sai, and H. Yugami, "100 nm period silicon antireflection structures fabricated using a porous alumina membrane mask," Appl. Phys. Lett. **78**, 142–143 (2001).
16. Q. Cao and P. Lalanne, "Negative role of surface plasmons in the transmission of metallic gratings with very narrow slits," Phys. Rev. Lett. **88**, 057403 (2002).
17. E. D. Palik, *Handbook of Optical Constants of Solids* (Academic, 1985).
18. J. P. Kottmann, O. J. F. Martin, D. R. Smith, and S. Schultz, "Plasmon resonances of silver nanowires with a nonregular cross section," Phys. Rev. B **64**, 235402 (2001).
19. S. M. Jang, D. Kim, S. H. Choi, K. M. Byun, and S. J. Kim, "Enhancement of localized surface plasmon resonance detection by incorporating metal–dielectric double-layered subwavelength gratings," Appl. Opt. **50**, 2846–2854 (2011).
20. X. D. Hoa, A. G. Kirk, and M. Tabrizian, "Towards integrated and sensitive surface plasmon resonance biosensors: a review of recent progress," Biosens. Bioelectron. **23**, 151–160 (2007).
21. C.-H. Choi and C.-J. Kim, "Fabrication of a dense array of tall nanostructures over a large sample area with sidewall profile and tip sharpness control," Nanotechnology **17**, 5326–5333 (2006).
22. J. M. Kontio, H. Husu, J. Simonen, M. J. Huttunen, J. Tommila, M. Pessa, and M. Kauranen, "Nanoimprint fabrication of gold nanocones with ~10 nm tips for enhanced optical interactions," Opt. Lett. **34**, 1979–1981 (2009).
23. S. Wang, D. F. P. Pile, C. Sun, and X. Zhang, "Nanopin plasmonic resonator array and its optical properties," Nano Lett. **7**, 1076–1080 (2007).
24. K. Ma, D. J. Kim, K. Kim, S. Moon, and D. Kim, "Target-localized nanograting-based surface plasmon resonance detection toward label-free molecular biosensing," IEEE J. Sel. Top. Quantum Electron. **16**, 1004–1014 (2010).
25. M. Piliarik and J. Homola, "Surface plasmon resonance (SPR) sensors: approaching their limits?," Opt. Express **17**, 16505–16517 (2009).